Earth and Planetary Science Letters 448 (2016) 34–41

Contents lists available at ScienceDirect

Earth and Planetary Science Letters

www.elsevier.com/locate/epsl

Final deglaciation of the Scandinavian Ice Sheet and implications for the Holocene global sea-level budget

Joshua K. Cuzzone [a,*], Peter U. Clark [b], Anders E. Carlson [b], David J. Ullman [b], Vincent R. Rinterknecht [c,j], Glenn A. Milne [d], Juha-Pekka Lunkka [e], Barbara Wohlfarth [f], Shaun A. Marcott [g], Marc Caffee [h,i]

[a] NASA Jet Propulsion Laboratory, California Institute of Technology, Pasadena, CA 91109, USA
[b] College of Earth, Ocean, and Atmospheric Science, Oregon State University, Corvallis, OR 97331, USA
[c] Université Paris 1 Panthéon-Sorbonne, Laboratoire de Géographie Physique, CNRS, UMR 8591, 92195 Meudon, France
[d] Department of Earth and Environmental Sciences, University of Ottawa, Ottawa, ON, Canada
[e] OMS-Glacial Sedimentology and Stratigraphy Group, P.O. Box 3000, FI-90014, University of Oulu, Oulu, Finland
[f] Department of Geological Sciences, University of Stockholm, Stockholm, Sweden
[g] Department of Geoscience, University of Wisconsin–Madison, Madison, WI 53706, USA
[h] Department of Physics and Astronomy, Purdue University, West Lafayette, IN 47907, USA
[i] Department of Earth, Atmospheric, and Planetary Sciences, Purdue University, West Lafayette, IN 47907, USA
[j] Department of Earth and Environmental Sciences, University of St Andrews, St Andrews KY16 9AL, UK

ARTICLE INFO

Article history:
Received 30 November 2015
Received in revised form 10 May 2016
Accepted 13 May 2016
Available online 24 May 2016
Editor: H. Stoll

Keywords:
sea level
ice sheets
Holocene

ABSTRACT

The last deglaciation of the Scandinavian Ice Sheet (SIS) from ~21,000 to 13,000 yr ago is well-constrained by several hundred ^{10}Be and ^{14}C ages. The subsequent retreat history, however, is established primarily from minimum-limiting ^{14}C ages and incomplete Baltic-Sea varve records, leaving a substantial fraction of final SIS retreat history poorly constrained. Here we develop a high-resolution chronology for the final deglaciation of the SIS based on 79 ^{10}Be cosmogenic exposure dates sampled along three transects spanning southern to northern Sweden and Finland. Combining this new chronology with existing ^{10}Be ages on deglaciation since the Last Glacial Maximum shows that rates of SIS margin retreat were strongly influenced by deglacial millennial-scale climate variability and its effect on surface mass balance, with regional modulation of retreat associated with dynamical controls. Ice-volume estimates constrained by our new chronology suggest that the SIS contributed ~8 m sea-level equivalent to global sea-level rise between ~14.5 ka and 10 ka. Final deglaciation was largely complete by ~10.5 ka, with highest rates of sea-level rise occurring during the Bølling–Allerød, a 50% decrease during the Younger Dryas, and a rapid increase during the early Holocene. Combining our SIS volume estimates with estimated contributions from other remaining Northern Hemisphere ice sheets suggests that the Antarctic Ice Sheet (AIS) contributed 14.4 ± 5.9 m to global sea-level rise since ~13 ka. This new constraint supports those studies that indicate that an ice volume of 15 m or more of equivalent sea-level rise was lost from the AIS during the last deglaciation.

1. Introduction

Understanding ice-sheet contributions to global sea-level rise since the Last Glacial Maximum (LGM) ~21,000 yr ago (21 ka) is important for establishing ice-sheet sensitivity to climate change (Church et al., 2013) as well as for constraining the signal of post-glacial isostatic adjustment (GIA) in estimates of current ice-sheet mass loss from the Gravity Recovery and Climate Experiment (GRACE) (Velicogna et al., 2014). The record of global mean sea-level (GMSL) rise is particularly well constrained for the last 13,000 yr (13 kyr) (Lambeck et al., 2014), but only the contributions of the North American Laurentide Ice Sheet (LIS) (Carlson et al., 2008; Simon et al., 2014; Ullman, 2013) and Greenland Ice Sheet (GIS) (Lecavalier et al., 2014) to this rise are well known. In contrast, the contributions of the Scandinavian Ice Sheet (SIS) (Hughes et al., 2015; Stroeven et al., 2015a) and Antarctic Ice Sheet (AIS) (Bentley et al., 2014; Carlson and Clark, 2012) during this time remain poorly constrained, largely due to insufficient and uncertain age control (Supplementary Material – see Comparison

* Corresponding author.
E-mail address: Joshua.K.Cuzzone@jpl.nasa.gov (J.K. Cuzzone).

http://dx.doi.org/10.1016/j.epsl.2016.05.019
0012-821X/

to existing age control), leaving a substantial component of the deglacial sea-level budget uncertain.

Here we develop a high-resolution chronology for the final deglaciation of the SIS based on new ^{10}Be cosmogenic exposure dates sampled along three transects spanning southern to northern Sweden and Finland. We then combine this new chronology with published ^{10}Be ages on deglaciation since the LGM to assess variations in the rate of ice-sheet retreat and their association with orbital- and millennial-scale climate change. We also derive develop ice-volume estimates constrained by our new chronology that allow us to derive the sea-level budget for ice-sheet contributions to GMSL since ~13 ka.

2. Methods

2.1. Field sampling methods

We sampled multiple erratic boulders for ^{10}Be dating at 16 sites along three transects across Sweden and Finland, with each transect beginning near the inferred Younger Dryas ice margin and converging to where flow lines indicate final SIS deglaciation in northwestern Sweden (Figs. 1, S1). Many areas in southern Sweden and Finland as well as near the Baltic Sea were submerged by the Baltic Ice Lake as it evolved towards the present-day Baltic Sea following isostatic uplift (Andrén et al., 2011). Accordingly, we only sampled above the highest shoreline to avoid shielding that would have otherwise taken place during post-glacial submersion. Sample preparation and beryllium isolation were performed at the Cosmogenic Isotope Laboratory at Oregon State University following standard laboratory protocols (Marcott, 2011; Rinterknecht et al., 2006) (Supplementary Information – see Sample processing).

Our three transects are perpendicular to inferred isochrones of SIS retreat established from regional ice-flow indicators or moraines (Johansson et al., 2011; Lunkka et al., 2004; Lundqvist, 1986). For transects 1 and 2, we include previously published ^{10}Be ages that extend coverage to the southern SIS position at the LGM (Fig. 1) (Table S2).

2.2. Correcting for uplift and changes in atmospheric thickness

We correct for post-glacial uplift and the associated time-varying effect on production rate. Many uplift corrections have used the nearest local relative sea level (RSL) curve to estimate uplift since ice retreat from that given location (Rinterknecht et al., 2006). Due to the large geographic spread of our sample sites, and the lack of RSL curves near most of them, extrapolating our sites to the nearest RSL curve would introduce unquantifiable, but potentially large, uncertainty. Moreover, changes in near-field RSL are influenced by the gravitational attraction of the ice sheet and thus over predict uplift at any given site (Clark, 1976).

To provide a consistent uplift correction history, we use the ICE-5G isostatic model of global ice cover during the last glacial cycle, which is coupled to the VM2 (with 90 km lithosphere) Earth model (Peltier, 2004). We have adopted ICE-5G rather than the more recent ICE-6G model (Peltier et al., 2015) because the loading history for the latter is only available from 26 ka. Predictions of deglacial land uplift are sensitive to the ice history prior to 26 ka given the response time of the mantle to surface loading. With regard to our use of ICE-5G (VM2) versus ICE-6G (VM5a), we note that results in Peltier et al. (2015; Fig. 14) indicate these models produce similar RSL curves for most localities in Fennoscandia. Thus, we are confident that our use of ICE-5G (VM2) will not significantly affect the results of this analysis.

The relative vertical land motion for each of our sites was generated using the theory described in Mitrovica et al. (1994) but upgraded to include the effect of Earth rotation (Mitrovica et al., 2005). Our isostatic model has a spatial resolution of ~50 km which is sufficient to capture spatial variability in the pattern of uplift (e.g. Bradley et al., 2011; Lambeck et al., 1998). This is largely because the Earth's lithosphere acts as a low-pass filter for surface-load-induced deformation.

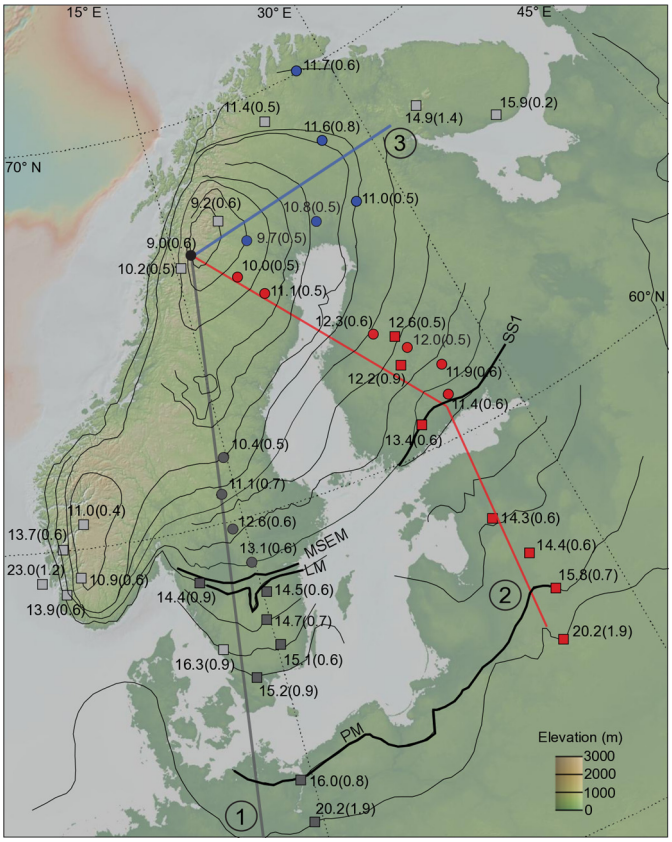

Fig. 1. ^{10}Be ages constraining the retreat history of the Scandinavian Ice Sheet. Site ^{10}Be ages are shown as either the arithmetic mean with their standard error or the error-weighted mean with their error-weighted uncertainty. Both methods for reporting uncertainty include the production rate uncertainty added in quadrature. Contours indicate isochrones of ice retreat (Johansson et al., 2011; Lunkka et al., 2004; Lundqvist, 1986). Colored lines indicate transects used for the time-distance diagram shown in Fig. 3. Circles indicate sites with ^{10}Be ages from the current study, and squares indicate sites with recalculated ^{10}Be ages (see Table S2); the colors of the circles and squares indicate the ages used for each transect (1: Sweden – dark gray, 2: Finland – red, 3: Northern Finland – blue). Light gray squares indicate additional ^{10}Be ages that constrain retreat history for areas beyond those represented by the transects. (For interpretation of the references to color in this figure legend, the reader is referred to the web version of this article.)

Uplift data are provided at 500-yr resolution (Tables S3, S4). We compute the time-averaged uplift for any particular site since the site became deglaciated. We estimate the time of initial deglaciation from our uncorrected ^{10}Be age. The site-averaged uplift is subtracted from the measured site elevation, and the corrected elevation is used to calculate the ^{10}Be age. This method yields results that are in excellent agreement with methods that calculate a time-dependent production rate given the elevation history (Brent Goehring, personal communication).

Young et al. (2013) noted that the uplift correction would be counteracted by changes in air pressure and associated production rate from retreating ice sheets, which has previously only been assessed for the LGM (Staiger et al., 2007). Lal (1991) found that cosmogenic isotope production rates can increase by up to 1% for every 10 m of elevation gain, given a 1.2 hPa drop in pressure. Because the climatic state throughout the last deglaciation varied in tandem with the rise in GMSL, pressure and mass distribution

globally would likely have differed during these time periods, thus altering cosmogenic isotope production. Using an atmosphere-only climate model, Staiger et al. (2007) found that climatic changes between the LGM and the present may have caused production rates to vary by up to 10%, although the largest influence occurred at high-elevation sites where the atmospheric mass varied greatly depending on the change in atmospheric temperature through time.

To assess the effect of changing atmospheric thickness on production rate, we used output from a coupled atmosphere-ocean general circulation model that simulated global climate at 3-kyr time intervals over the last 21 kyr (Alder and Hostetler, 2014). We used surface pressure and temperature at our given site locations, interpolated to the same resolution as the modeled uplift (500 yr). We use the hypsometric equation (1) to determine changes in the atmospheric thickness between our time intervals compared to present day. Classically, the hypsometric equation is used to determine the thickness (in meters) between two isobaric (pressure) surfaces given the mean temperature of the layer. The hypsometric equation is:

$$h = \frac{R\overline{T}}{g} \ln\left(\frac{p_1}{p_2}\right) \tag{1}$$

where the atmospheric thickness (h) between two layers is related to the mean temperature of that layer, p_1 and p_2 are the surface pressure at each time interval, $\overline{T}$ is the mean surface temperature between the particular time intervals, R is the gas constant for dry air, and g is gravity.

Rather than calculating the thickness change of the whole atmospheric column between time intervals, we take the mean temperature of our layer to be the mean surface temperature between a given time interval and present day. Accordingly, the surface pressures for that given time interval and present are used. For example, the climate at 21 ka was much colder than present over the SIS, and thus the atmosphere was thinner. By calculating the thickness change using surface temperature and pressure between 21 ka and present, we can evaluate what the atmospheric thickness difference would be at the LGM compared to present. During the LGM, the atmosphere was colder and surface pressures were thus higher at our sites (Alder and Hostetler, 2014). Because atmospheric pressure was higher relative to present, this would be equivalent to our present-day site being lower in elevation to obtain a higher surface pressure. Because of this effect, production would be lower during this colder interval, due to higher surface pressure relative to present. Using the hypsometric equation, this change in height can be evaluated. We find that the climate effect at all of our sites is small, equivalent to ~4% change in the uplift correction, and its effect on the overall age of our sites is to shift ages only 1–2% older. Therefore, we exclude this correction from the overall correction, and only account for the larger effect of post-glacial uplift.

2.3. ^{10}Be production rate and age calculation

We calculated individual surface exposure ages using a revised western Norway production rate (Goehring et al., 2012b) that, because of its proximity to our sites, makes it more applicable than other calibration data sets that are geographically further away. The western Norway production rate is based on two calibration sites: a Younger Dryas end moraine at Halsnøy and a mid-Holocene rock avalanche at Oldedalen. Using a nearby RSL curve to correct for post-glacial uplift at the Halsnøy site, and assuming no uplift at the Oldedalen site, Goehring et al. (2012b) calculated the combined production rate as 4.15 ± 0.15 atoms g^{-1} yr^{-1} (all production rates discussed in this section are based on the Lal/Stone scaling) (Balco et al., 2008). We derive an uplift-corrected combined production rate for the Halsnøy and Oldedalen sites of 4.29 ± 0.14 atoms g^{-1} yr^{-1}, as both sites have undergone isostatic uplift following deglaciation, similar to the combined production rate derived by Goehring et al. (2012a) and a recently derived production rate from a site in southern Sweden (4.19 ± 0.20 atoms g^{-1} yr^{-1}, non-uplift corrected) (Stroeven et al., 2015b).

For comparison, the non-uplift corrected Arctic production rate is 3.96 ± 0.15 atoms g^{-1} yr^{1} and the uplift-corrected rate is 4.16 ± 0.19 atoms g^{-1} yr^{-1} (Young et al., 2013). Young et al. (2013) assessed their two production rates by comparing the scatter of the associated predicted ages versus true ages for several different calibration sites. The difference in scatter between the two approaches, as measured by the standard deviation, was ~1%, with the non-uplift corrected value having the smaller standard deviation (5.2%). On the basis of this "slightly better" fit, as well as agreement of their non-uplift corrected production rate with the value reported from the Oldedalen site (4.04 ± 0.13 atoms g^{-1} yr^{-1}) (Goehring et al., 2012b), which they suggested experienced relatively little uplift, Young et al. (2013) recommend using the non-uplift corrected value. If an uplift-corrected value is used, they suggest that it must include the time-varying effect of uplift on production rate.

We apply an uplift correction to the western Norway production rate for the following reasons. First, we do not assign any significance to the ~1% difference in standard deviation that Young et al. (2013) used to support a non-uplift correction. Second, the non-uplift corrected Arctic production rate (3.96 ± 0.15 atoms g^{-1} yr^{-1}) that is based on sites that experienced uplift is less similar to the Oldedalen-site production rate when corrected for uplift (4.08 ± 0.13 atoms g^{-1} yr^{-1} based on our correction), and the uplift-corrected Arctic production rate (4.16 ± 0.19 atoms g^{-1} yr^{-1}) is similar to the uplift-corrected western Norway production rate (4.29 ± 0.14 atoms g^{-1} yr^{-1}) based on our uplift correction.

We use the Lal–Stone time-varying (Lm) scaling scheme (Lal, 1991; Stone, 2000) for the presentation of our ages, although using other scaling schemes (Desilets et al., 2006; Dunai, 2001; Lifton et al., 2008) does not significantly alter the results or interpretations of our ages. All previously published ^{10}Be chronologies used in our compilation are recalculated using our revised western Norway production rate (Table S2), thus producing a standardized ^{10}Be data set encompassing the entire deglaciation of the SIS from its southern LGM limit to its final demise in northwestern Sweden.

We identify five samples with ages that are three or more standard deviations outside of the site mean as outliers (Table S4). We also identified eight statistical outliers using Chauvenet's criterion (Table S4), conditioned by samples that have <50% probability of falling within the normal distribution of the sample population following Rinterknecht et al. (2006). Before calculating site ages, we tested if our samples fall within a normally distributed population using a Shapiro–Wilk test for normality.

In order to report the most conservative estimate of site age and uncertainty, we first assess the geologic uncertainty and analytic uncertainty of our sample populations (Rinterknecht et al., 2006). The geologic uncertainty is defined as the standard deviation of the boulder ages for each given site. This is compared to the analytic uncertainty, defined by the average site internal uncertainty, which reflects the measurement uncertainty. In the case where the geologic uncertainty is larger than the analytic uncertainty, the site age is defined by the arithmetic mean of the sample population and the standard error of the ages. Conversely, where the analytic uncertainty is larger than the geologic uncertainty, we define the site age as the error-weighted mean of the sample population and the error-weighted uncertainty (of the internal uncertainty). Although this approach provides the most conservative estimate of site age and uncertainty, the differences between them are negligible. For 14 of our 16 sites, the ages from the two

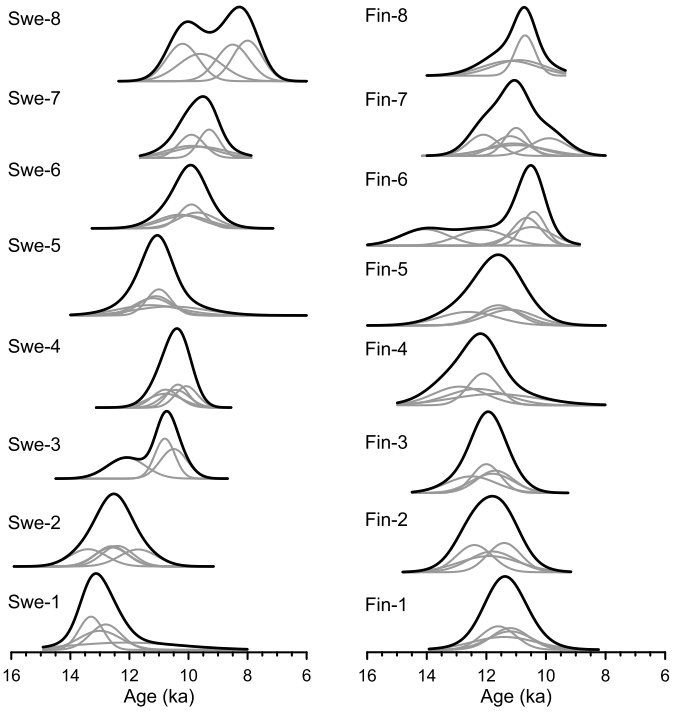

Fig. 2. Probability distribution functions (PDFs) of ^{10}Be ages for our site locations in Finland and Sweden shown in Figs. 1 and S1. Red lines are individual ages, and black lines are cumulative PDFs. (For interpretation of the references to color in this figure legend, the reader is referred to the web version of this article.)

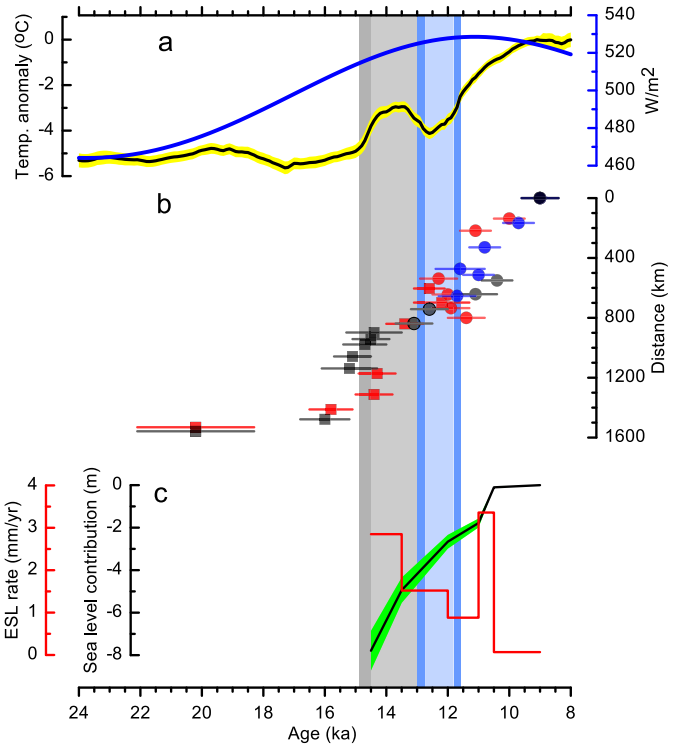

Fig. 3. Retreat history of the Scandinavian Ice Sheet since the Last Glacial Maximum and its relation to climate. **a.** June insolation at 65°N (Berger et al., 1993) and temperature anomaly and 1-sigma uncertainty for 90–30°N (Marcott et al., 2013; Shakun et al., 2012). **b.** Time-distance diagram showing retreat along three transects shown in Fig. 1. Gray symbols correspond to transect 1, red symbols correspond to transect 2, and blue symbols correspond to transect 3. The black symbol represents the common termination point in northwestern Sweden (Fig. 1). **c.** The sea-level contribution from the Scandinavian Ice Sheet, and the corresponding rate of sea-level contribution. The shading indicates the 12% uncertainty associated with the conversion of ice area to volume. The gray vertical rectangle corresponds to the Bølling–Allerød warm interval, with the dark gray rectangle indicating the 2-sigma uncertainty for its onset (Rasmussen et al., 2006). The blue rectangle corresponds to the Younger Dryas cold interval, with the dark blue rectangles indicating the 2-sigma uncertainty for its onset and termination (Rasmussen et al., 2006). (For interpretation of the references to color in this figure legend, the reader is referred to the web version of this article.)

methods differ by 0–2%, or a difference of 0 to 200 yr, which is well within the uncertainty. Only two sites (Fin-6 and Swe-8) have larger differences (3% and 5% respectively), but again, these are within the uncertainty of the ages. Lastly, the production rate uncertainty is added to the calculated uncertainties in quadrature.

In the case of our site mean ages, we assume that all ages in each of those populations date the same retreat of the SIS from that given location. We represent each age as a probability distribution function (PDF), given by the equation:

$$y = \frac{1}{\sqrt{2\pi\sigma^2}} \exp\left[\frac{-(x-\mu)^2}{2\sigma^2}\right] \quad (2)$$

where μ is the mean and σ is the standard deviation. We then sum all individual PDFs to obtain the cumulative PDF, which allows for a representation of the maximum likelihood of the particular site age, given the individual distributions of each sample (Fig. 2).

Other than sites Swe-3, Swe-8, and Fin-6, all sites have a single peak in their cumulative PDF (Fig. 2). Many of the individual frequency distributions from each site overlap, providing confidence that each sample is measuring the same deglacial event of the SIS.

3. Results

Recalculated ^{10}Be ages suggest that retreat from the southern SIS LGM margin began 20.2 ± 1.9 ka (Figs. 1, 3), consistent with the termination of the global LGM (Clark et al., 2009). Our new ^{10}Be ages indicate that final deglaciation of the SIS occurred in northwestern Sweden at 9.0 ± 0.6 ka (Fig. 1). Fig. 3 compares the new SIS retreat history to 65°N summer insolation (Berger et al., 1993) and a reconstruction of 30–90°N temperature (Marcott et al., 2013; Shakun et al., 2012) in order to evaluate the relation between ice-margin retreat and deglacial climate change. Throughout the deglaciation, each transect shows similar variations in ice-margin retreat rates (Fig. 3b), indicating coherent SIS-wide responses to climate forcing. Based on the chronology derived from the recalculated ^{10}Be ages, the southern SIS margin retreated slowly from its LGM position (20.2 ± 1.9 ka) to the first major recessional moraine across the Baltic plain before 16.0 ± 0.8 ka (Pomeranian moraine) (Figs. 1, 3). Climate modeling indicates that this early retreat was likely in response to the corresponding increase in high-latitude summer insolation and associated snow-albedo feedback (He et al., 2013).

A significant increase in retreat rates along transect 1 occurred between 16.0 ± 0.8 ka and 15.2 ± 0.9 ka (Fig. 3b) as the margin retreated north across the Baltic Sea (Fig. 1). Although, the Norwegian Ice Stream began to break up ~20 ka (Svendsen et al., 2015), Larsen et al. (2012) attribute this retreat across southwest Sweden to a dynamical control associated with the drawdown by the Norwegian Channel ice stream. The recalculated ^{10}Be ages from southernmost Sweden are in agreement with minimum-limiting ^{14}C and varve ages in showing a subsequent reduction in retreat rates during the Bølling–Allerød warm period (Fig. 3b). In contrast, retreat rates along transect 2 remain slow until a significant increase at the onset of the Bølling–Allerød warm period (Fig. 3b), indicating that retreat of this sector was largely influenced by a temperature control on surface mass balance.

Our new chronology for sites along transect 1 extends the SIS retreat history from southern Sweden to the site of final deglaciation in the northwestern Swedish highlands (Fig. 1). Retreat from our first sampled site (Swe-1) at 13.1 ± 0.6 ka to the next site

along this transect (Swe-2) suggests continued moderate rates of ice-margin retreat during the Bølling–Allerød, while the age from Swe-3 (11.1 ± 0.7 ka) suggests a reduction in rate during the Younger Dryas (Fig. 3). We note, however, that our ages for Swe-1 and Swe-2 suggest a considerably older age for retreat for this region than traditionally inferred based on multiple lines of evidence, which places the ice margin further south at those times and suggests that retreat rates immediately following the Younger Dryas would be higher than what we show (Supplementary Information – see Comparison to existing age control).

Our remaining ages on this transect indicate that rapid ice-margin retreat then resumed during the early Holocene until final deglaciation at 9.0 ± 0.6 ka (Swe-8). This response to early Holocene warming likely reflects a large rise of the SIS equilibrium line altitude, with an initial episode of rapid ice loss through high ablation rates below the equilibrium line followed by diminishing rates of loss as the ice margin retreated to higher elevations, decreasing the ablation area.

On transect 2, the recalculated age of the Salpausselkä I moraine (SSI) in southeastern Finland (13.4 ± 0.6 ka) and our new age from the Salpausselkä II moraine (SSII) (11.4 ± 0.6 ka), <50 km up ice from the SSI moraine, suggest a slower retreat rate during the Younger Dryas (Fig. 3b). The SSII age and the next three ages on this transect are all within uncertainty of each other, indicating rapid, near-instantaneous retreat of the SIS southeastern margin, similar to rapid retreat of the Swedish margin along transect 1. Within uncertainties, however, this episode of rapid retreat across southern Finland corresponds to the abrupt warming that marks the start of the Holocene at ~11.7 ka, whereas the retreat across southern Sweden occurred a few hundred years later (Fig. 3b). We suggest that this earlier retreat relative to the Swedish margin may reflect an additional dynamical contribution of mass loss from calving and sub-lacustrine melting in the proglacial lake that was in contact with much of the Finnish margin during this period of retreat (Björck, 1995), thus reducing the response time to early Holocene warming. Ages from the remaining two sites on transect 2 then show that retreat from the Swedish coast (11.1 ± 0.5 ka) proceeded at a relatively slow rate over the final ~200 km until final deglaciation at 9.0 ± 0.6 ka.

Transect 3 begins at a site within an inferred Younger Dryas moraine complex (Johansson et al., 2011), which is confirmed by our age for this site (11.7 ± 0.6 ka). Our age from site Fin-6 (11.6 ± 0.8 ka) and an adjacent site (11.4 ± 0.5 ka) (Stroeven et al., 2011) along with our remaining ages from this transect suggest similar retreat rates as for transect 1 (Fig. 3b).

4. Comparison to existing age control

In general, our new chronology is in good agreement with the few existing ^{14}C and ^{10}Be ages that closely constrain the time of deglaciation (Figs. 1, 3) (Supplementary Information – see Comparison to existing age control). However, there is a considerable difference in the age of the Middle Swedish End Moraines (MSEMs) in southern Sweden. Our first two sites on transect 1 (Swe-1 and Swe-2) are north of the MSEMs. The mean ^{10}Be ages from these sites, which are in stratigraphic order with mean ^{10}Be ages to the south and north, suggest that ice had retreated from the MSEMs before 13.1 ± 0.6 ka. However, this is in conflict with the age of the MSEMs according to the standard deglaciation model of Sweden, which suggests that they formed later during the Younger Dryas period (Björck, 1995; Lundqvist, 1986; Lundqvist and Wohlfarth, 2001; Wohlfarth et al., 2008). There is currently no *a priori* reason, however, to dismiss either of the age interpretations (Supplementary Information – see Comparison to existing age control). Until further age control becomes available involving dating the MSEMs directly or obtaining additional ages to the north of the MSEMs near our sites Swe-1 and Swe-2, we propose that both scenarios are equally viable. The first scenario, based on our mean ^{10}Be ages from sites Swe-1 and Swe-2, suggests a more gradual retreat from the MSEMs, as suggested by the mean ^{10}Be age of the Levene Moraine immediately to the south of the MSEMs (14.4 ± 0.9 ka) (Larsen et al., 2012) and the mean ^{10}Be age for site Swe-1 (13.1 ± 0.6 ka). In contrast, a Younger Dryas age for the MSEMs suggests that our mean ^{10}Be ages from sites Swe-1 and Swe-2 are too old and should be dismissed. In this case, retreat from the MSEMs at the end of the Younger Dryas (~11.7 ka) to site Swe-3 further north on transect 1 (11.1 ± 0.7 ka) (Fig. 1) suggests a more rapid rate of retreat immediately at the end of the Younger Dryas. Given that we are dealing with a very small fraction of the total SIS area at this time, we note that adopting either result does not change our conclusions below regarding the contribution of SIS to global sea level.

Hughes et al. (2015) and Stroeven et al. (2015a) recently compiled published ^{14}C, ^{10}Be, and varve ages in their syntheses of the last deglaciation of the SIS, which are also included in our compilation (Fig. S2). All other ^{14}C ages in their compilations are minimum-limiting ages that substantially post-date deglaciation. Stroeven et al. (2015b) also reported 132 new ^{10}Be ages on sand, cobbles, pebbles, boulders, and bedrock. Of these, we only included ages from sites that are directly comparable to our sample protocols (three or more ages on boulders from a site, screened for outliers). On this basis, we included seven ages from two sites in south-central Finland, which are in agreement with our ages on transect 2 (Figs. 1, 3b), and six ages from two sites on the Kola Peninsula (Fig. 1; Table S2).

5. Estimate of ice-volume and sea-level contributions

We estimate the SIS volume and equivalent GMSL contribution beginning at ~14.5 ka and continuing through the remainder of the deglaciation using our newly established chronology. We divide the SIS deglaciation into five time periods when we have the best age control on the full extent of the ice area: 14.5 ka, 13.5 ka, 12.0 ka, 11.0 ka, 10.5 ka, and final deglaciation at 9.0 ka (Fig. S2). We are unable to extend the volume estimates older than ~14.5 ka as there is limited chronology for the SIS retreat for the Barents Sea and western Russia regions. The areas drawn are bounded by the nearest age constraint at particular sites. Where there are no ages to constrain the area, we follow mapped isochrones (Boulton et al., 2001; Johansson et al., 2011; Lundqvist, 1986) to the site closest in age to the particular area interval being drawn.

To estimate the ice volume, we use the area-volume scaling relation (Paterson, 1972):

$$\log(V) = 1.23\big(\log(A) - 1\big) \tag{3}$$

where V is ice volume in km^3, and A is ice areal extent in km^2, with an uncertainty on the resulting ice volume (V) of ±12%. Although this assumes that an ice sheet or ice cap is in equilibrium, this relationship was developed on ice sheets and ice caps in different mass balance states (both positive and negative) with single and multiple ice domes. These ice sheets and ice caps span four orders of magnitude in area (Antarctic Ice Sheet to the Barnes Ice Cap) and climate conditions from temperate maritime (Iceland) to polar desert (Antarctica). This relationship assumes that the ice sheet is resting on a hard bed with all ice motion by internal ice deformation, making this a maximum estimate for volume. We convert calculated ice volumes to equivalent GMSL by dividing a given volume by the global ocean area at each time period as determined by the ICE-5G model (Peltier, 2004), accounting for the density of ice (917 kg m^{-3}) and seawater (1,027 kg m^{-3}).

We estimate that the SIS contributed 7.8 ± 1.0 m to GMSL from 14.5 ka until final deglaciation at ~9.1 ka, with all but ~0.1 m

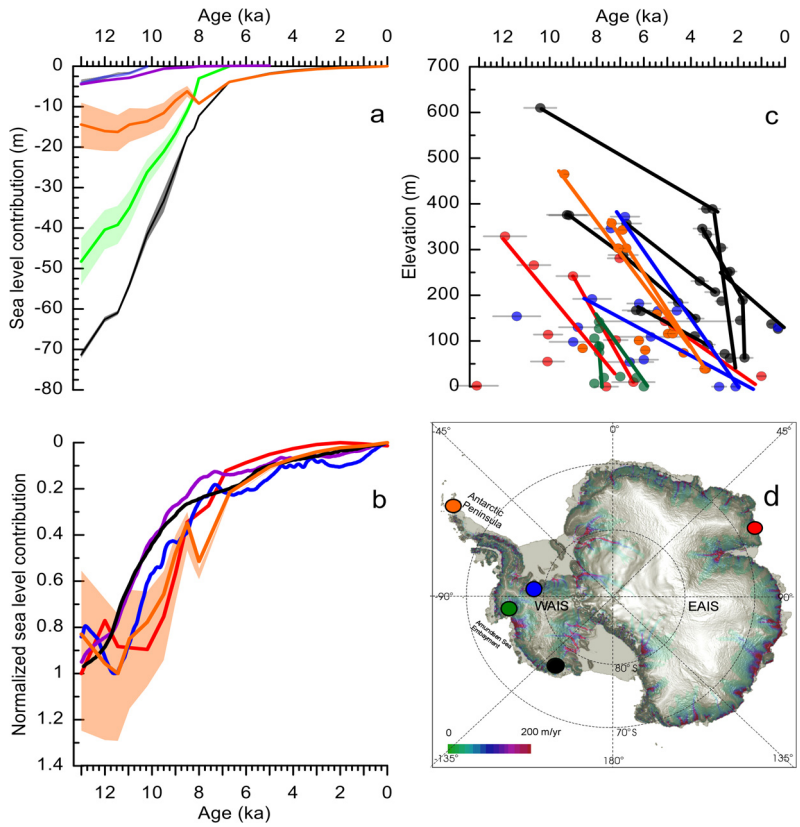

Fig. 4. a. Sea-level contribution from the Scandinavian Ice Sheet (SIS) (blue) (current study), Laurentide Ice Sheet (LIS) (green) (Carlson et al., 2008; Dyke, 2004; Ullman, 2013), and Greenland Ice Sheet (GIS) (magenta) (Lecavalier et al., 2014). The residual (orange) is the difference between the sum of the Northern Hemisphere ice sheets (SIS + LIS + GIS) and global mean sea level (black) (Lambeck et al., 2014). **b**. Estimates of the sea-level equivalent contribution from the Antarctic Ice Sheet for the period ~13 ka to present, normalized to total contribution at ~13 ka. The orange line (Carlson et al., 2008; Dyke, 2004; Ullman, 2013) and the red line (Tarasov et al., 2012) were calculated as the residual of the sum of the Northern Hemisphere sources of sea-level rise subtracted from global mean sea-level rise (Lambeck et al., 2014). The black (Briggs et al., 2014), magenta (Golledge et al., 2014), and blue (Golledge et al., 2014) lines are from ice-sheet modeling; the blue shading is the 1-sigma uncertainty for the black line. Although the total contribution from Antarctica at 13 ka varies between the reconstructions, the shape of the curves is similar, indicating consistency in the timing of the Antarctic contribution to global-mean sea-level rise across all reconstructions. **c.** ^{10}Be ages for Antarctic Ice Sheet surface-elevation change (see Table S6). Error shown is the reported 1-sigma uncertainty. Lines show the corresponding published trends for ice-surface lowering based on for sample populations. **d.** Map of Antarctica showing location of sites with ^{10}Be ages shown in panel C, with same color coding. (For interpretation of the references to color in this figure legend, the reader is referred to the web version of this article.)

lost by ~10.5 ka. This contribution is ~2 m greater than estimated by GIA models (Lambeck et al., 2010; Peltier, 2004), but the same as in the recent DATED reconstruction (Hughes et al., 2015) and within ~0.7 m of the value derived by applying our approach to the reconstruction of areal extent by Stroeven et al. (2015a) (Fig. S3). Our reconstruction differs from these latter two reconstructions, however, in showing higher rates of mass loss during the Bølling–Allerød and early Holocene, such that the SIS was largely gone by ~10.5 ka (Fig. 3c) as compared to 2–3 m still remaining at this time in these other reconstructions (Fig. S3).

Fig. 4a combines the SIS sea-level contribution with the contributions from the LIS (Carlson et al., 2008; Dyke, 2004; Ross et al., 2012; Simon et al., 2014; Ullman, 2013) and GIS (Lecavalier et al., 2014) since ~13 ka, corresponding to the period when GMSL is best constrained by sea-level data (Lambeck et al., 2014); other Northern Hemisphere ice sheets had disappeared by this time (Clark et al., 2012; Dyke, 2004). The LIS, SIS, and GIS contributions then constitute the Northern Hemisphere contribution to GMSL rise since ~13 ka. We subtract this Northern Hemisphere ice-sheet contribution from GMSL to derive a residual sea-level contribution of 14.4 ± 5.9 m since 13 ka. We derive a higher residual of 26.9 ± 3.3 m using an alternative reconstruction for the North American ice sheet, which includes a small contribution from the Cordilleran Ice Sheet (CIS) as well as the LIS (Tarasov et al., 2012) (Fig. S4). Because mountain glaciers globally were largely at their present-day extent by 13–14 ka (Shakun et al., 2015), the AIS is the only other significant source of mass loss since ~13 ka.

Our AIS estimate of sea-level rise since 13 ka is comparable to that derived by the ICE-6G model (13.6 m since 14 ka) (Argus et al., 2014), and consistent with those studies that indicate that an equivalent GMSL rise of 20 m or more was lost from the AIS during the last deglaciation (Lambeck et al., 2014), but is substantially greater than other recent models that suggest a contribution of only 2.5–8.0 m during the last deglaciation (Briggs et al., 2014; Golledge et al., 2014; Ivins et al., 2013; Whitehouse et al., 2012). Despite the differences in the total amount, our result suggesting that a substantial AIS contribution to GMSL rise occurred after 13 ka is consistent with the timing found in most AIS model reconstructions (Argus et al., 2014; Briggs et al., 2014; Golledge et al., 2014; Ivins et al., 2013) (Fig. 4b) as well as with evidence for widespread ice-surface lowering (Fig. 4c, d), and with evidence from far-field relative sea-level sites (Mauz et al., 2015). The wide range in the volume of the AIS reconstructions largely reflects uncertainties in the paleodata constraints on ice-sheet models (Carlson and Clark, 2012) and in the viscosity and lateral heterogeneity of the mantle on GIA models (Wu and Van der Wal, 2003; Paulson et al., 2005; van der Wal et al., 2015). Resolving the discrepancy between AIS reconstructions is central to balancing the GMSL budget during and

following the LGM (Clark and Tarasov, 2014; Lambeck et al., 2014) and to producing accurate estimates of present-day AIS mass loss from GRACE (Velicogna et al., 2014) and Ice, Cloud and land Elevation Satellite (Zwally et al., 2015) measurements.

6. Conclusions

Our new ^{10}Be chronology provides a significant improvement in constraining the timing of deglaciation of the SIS since 13 ka. Our chronology shows largely good agreement with existing age control that closely constrains the time of final deglaciation as ~9.1 ka. Combining this new chronology with existing ^{10}Be ages on deglaciation since the LGM provides a comprehensive, standardized ^{10}Be data set encompassing the entire deglaciation of the SIS from its southern LGM limit to its final demise in northwestern Sweden. This new chronology shows that rates of SIS margin retreat were strongly influenced by deglacial millennial-scale climate variability and its effect on surface mass balance, with regional modulation of retreat associated with dynamical controls. We use our estimate of the contribution of SIS mass loss to GMSL to close the budget for the Northern Hemisphere ice-sheet contribution to GMSL since 13 ka. Subtracting this contribution from the record of GMSL suggests that the AIS contributed 14.4 ± 5.9 m to sea-level rise since 13 ka, which is considerably more than that suggested by most recent models of AIS deglaciation.

Author Contributions

P.U.C. and A.E.C. conceived the study. J.K.C, P.U.C, J.P.L and B.W. conducted field sampling. J.K.C. and S.A.M. performed laboratory procedures; J.K.C, P.U.C, S.A.M, and V.R.R. calculated ^{10}Be exposure ages and site averages. J.K.C., D.J.U., A.E.C., P.U.C. gathered data to reconstruct sea-level estimates. G.A.M. provided output for uplift corrections. M.C. supervised ^{10}Be measurements using Accelerator Mass Spectrometry at the PRIME lab. J.K.C. and P.U.C. wrote the manuscript, with input from all authors.

Acknowledgements

We thank Jay Alder, Aaron Barth, Andrea Balbas, Nilo Bill, Svante Björck, Akkaneewut Chabangborn, Brent Goehring, Nat Lifton, and Jukka-Pekka Palmu for help and discussions related to this project, Jonathan Bamber for the base map used in Fig. 3d, and the two journal reviewers for their helpful comments. Research was supported by a GSA graduate student research grant to JKC, NSF grant EAR-0958417 to PUC, and NSF grants EAR-0958872 and EAR-1343573 to AEC. PRIME Lab is supported by NSF grant EAR-0844151.

Appendix A. Supplementary material

Supplementary material related to this article can be found online at http://dx.doi.org/10.1016/j.epsl.2016.05.019.

References

Alder, J., Hostetler, S.W., 2014. Global climate simulations at 3000 year intervals for the last 21 000 years with the GENMOM coupled atmosphere–ocean model. Clim. Past Discuss. 10, 2925–2978.

Andrén, T., Björck, S., Andrén, E., Conley, D., Zillén, L., Anjar, J., 2011. The development of the Baltic Sea basin during the last 130 ka. In: Harff, J., Björck, S., Hoth, P. (Eds.), The Baltic Sea Basin. Springer, Berlin, pp. 75–97.

Argus, D.F., Peltier, W.R., Drummond, R., Moore, A.W., 2014. The Antarctica component of postglacial rebound model ICE-6G_C (VM5a) based on GPS positioning, exposure age dating of ice thicknesses, and relative sea level histories. Geophys. J. Int. 198, 537–563.

Balco, G., Stone, J.O., Lifton, N.A., Dunai, T.J., 2008. A complete and easily accessible means of calculating surface exposure ages or erosion rates from Be-10 and Al-26 measurements. Quat. Geochronol. 3, 174–195.

Bentley, M.J., Cofaigh, C.O., Anderson, J.B., Conway, H., Davies, B., Graham, A.G.C., Hillenbrand, C.D., Hodgson, D.A., Jamieson, S.S.R., Larter, R.D., Mackintosh, A., Smith, J.A., Verleyen, E., Ackert, R.P., Bart, P.J., Berg, S., Brunstein, D., Canals, M., Colhoun, E.A., Crosta, X., Dickens, W.A., Domack, E., Dowdeswell, J.A., Dunbar, R., Ehrmann, W., Evans, J., Favier, V., Fink, D., Fogwill, C.J., Glasser, N.F., Gohl, K., Golledge, N.R., Goodwin, I., Gore, D.B., Greenwood, S.L., Hall, B.L., Hall, K., Hedding, D.W., Hein, A.S., Hocking, E.P., Jakobsson, M., Johnson, J.S., Jomelli, V., Jones, R.S., Klages, J.P., Kristoffersen, Y., Kuhn, G., Leventer, A., Licht, K., Lilly, K., Lindow, J., Livingstone, S.J., Masse, G., McGlone, M.S., McKay, R.M., Melles, M., Miura, H., Mulvaney, R., Nel, W., Nitsche, F.O., O'Brien, P.E., Post, A.L., Roberts, S.J., Saunders, K.M., Selkirk, P.M., Simms, A.R., Spiegel, C., Stolldorf, T.D., Sugden, D.E., van der Putten, N., van Ommen, T., Verfaillie, D., Vyverman, W., Wagner, B., White, D.A., Witus, A.E., Zwartz, D., Consortium, R., 2014. A community-based geological reconstruction of Antarctic Ice Sheet deglaciation since the Last Glacial Maximum. Quat. Sci. Rev. 100, 1–9.

Berger, A., Loutre, M.F., Tricot, C., 1993. Insolation and Earth's orbital periods. J. Geophys. Res. 98, 10341–10362.

Björck, S., 1995. A review of the history of the Baltic Sea, 13.0–8.0 ka BP. Quat. Res. 27, 19–40.

Boulton, G.S., Dongelmans, P., Punkari, M., Broadgate, M., 2001. Palaeoglaciology of an ice sheet through a glacial cycle: the European ice sheet through the Weichselian. Quat. Sci. Rev. 20, 591–625.

Bradley, S.L., Milne, G.A., Shennan, I., Edwards, R., 2011. An improved glacial isostatic adjustment model for the British Isles. J. Quat. Sci. 26, 541–552.

Briggs, R.D., Pollard, D., Tarasov, L., 2014. A data-constrained large ensemble analysis of Antarctic evolution since the Eemian. Quat. Sci. Rev. 103, 91–115.

Carlson, A.E., Clark, P.U., 2012. Ice sheet sources of sea level rise and freshwater discharge during the last deglaciation. Rev. Geophys. 50, RG4007.

Carlson, A.E., Legrande, A.N., Oppo, D.W., Came, R.E., Schmidt, G.A., Anslow, F.S., Licciardi, J.M., Obbink, E.A., 2008. Rapid early Holocene deglaciation of the Laurentide ice sheet. Nat. Geosci. 1, 620–624.

Church, J.A., Clark, P.U., Cazenave, A., Gregory, J.M., Jevrejeva, S., Levermann, A., Merrifield, M.A., Milne, G.A., Nerem, R.S., Nunn, P.D., Payne, A.J., Pfeffer, W.T., Stammer, D., Unnikrishnan, A.S., 2013. Sea level change. In: Stocker, T.F., Qin, D., Plattner, G.-K., Tignor, M., Allen, S.K., Boschung, J., Nauels, A., Xia, Y., Bex, V., Midgley, P.M. (Eds.), Climate Change 2013: The Physical Science Basis. Contribution of Working Group I to the Fifth Assessment Report of the Intergovernmental Panel on Climate Change. Cambridge University Press, Cambridge, United Kingdom and New York, NY, USA, pp. 1137–1216.

Clark, J., McCabe, A.M., Bowen, D.Q., Clark, P.U., 2012. Response of the Irish Ice Sheet to abrupt climate change during the last deglaciation. Quat. Sci. Rev. 35, 100–115.

Clark, J.A., 1976. Greenland's rapid postglacial emergence: a result of ice–water gravitational attraction. Geology 30, 310–312.

Clark, P.U., Dyke, A.S., Shakun, J.D., Carlson, A.E., Clark, J., Wohlfarth, B., Mitrovica, J.X., Hostetler, S.W., McCabe, A.M., 2009. The last glacial maximum. Science 325, 710–714.

Clark, P.U., Tarasov, L., 2014. Closing the sea level budget at the Last Glacial Maximum. Proc. Natl. Acad. Sci. USA 111, 15861–15862.

Desilets, D., Zreda, M.G., Prabu, T., 2006. The energy dependence of cosmogenic nuclide scaling models: new measurements at low latitudes. Earth Planet. Sci. Lett. 246, 265–276.

Dunai, T.J., 2001. Influence of secular variation of the geomagnetic field on the production rates of in situ produced cosmogenic nuclides. Earth Planet. Sci. Lett. 193, 197–212.

Dyke, A.S., 2004. An outline of North American deglaciation with emphasis on central and northern Canada. In: Ehlers, J., Gibbard, P.L. (Eds.), Quaternary Glaciations: Extent and Chronology. Elsevier, Amsterdam, pp. 373–424.

Goehring, B.M., Lohne, O.S., Mangerud, J., Svendsen, J.I., Gyllencreutz, R., Schaefer, J., Finkel, R., 2012a. Late glacial and Holocene ^{10}Be production rates for western Norway. J. Quat. Sci. 27, 89–96.

Goehring, B.M., Lohne, O.S., Mangerud, J., Svendsen, J.I., Gyllencreutz, R., Schaefer, J., Finkel, R., 2012b. Late Glacial and Holocene ^{10}Be production rates for western Norway: erratum. J. Quat. Sci. 27, 544.

Golledge, N.R., Menviel, L., Carter, L., Fogwill, C.J., England, M.H., Cortese, G., Levy, R.H., 2014. Antarctic contribution to meltwater pulse 1A from reduced Southern Ocean overturning. Nat. Commun. 5, 5107.

He, F., Shakun, J.D., Clark, P.U., Carlson, A.E., Liu, Z., Otto-Bliesner, B.L., Kutzbach, J.E., 2013. Northern Hemisphere forcing of the last deglaciation in the Southern Hemisphere. Nature 494, 81–85.

Hughes, A.L.C., Gyllencreutz, R., Lohne, Ø.S., Mangerud, J., Svendsen, J.I., 2015. The last Eurasian ice sheets – a chronological database and time-slice reconstruction. DATED-1. Boreas.

Ivins, E.R., James, T.S., Wahr, J., Schrama, E.J.O., Landerer, F.W., Simon, K.M., 2013. Antarctic contribution to sea level rise observed by GRACE with improved GIA correction. J. Geophys. Res., Solid Earth 118, 1–16.

Johansson, P., Lunkka, J.P., Sarala, P., 2011. Glaciation of Finland. In: Ehlers, J., Gibbard, P.L., Hughes, P.D. (Eds.), Developments in Quaternary Science. Elsevier, Amsterdam, The Netherlands, pp. 105–116.

Lal, D., 1991. Cosmic ray labeling of erosion surfaces: in-situ nuclide production rates and erosion models. Earth Planet. Sci. Lett. 104, 424–439.

Lambeck, K., Purcell, A., Zhao, J., Svensson, N.O., 2010. The Scandinavian Ice Sheet: from MIS 4 to the end of the Last Glacial Maximum. Boreas 39, 410–435.
Lambeck, K., Rouby, H., Purcell, A., Sun, Y., Sambridge, M., 2014. Sea level and global ice volumes from the Last Glacial Maximum to the Holocene. Proc. Natl. Acad. Sci. USA 111, 15296–15303.
Lambeck, K., Smither, C., Johnston, P., 1998. Sea-level change, glacial rebound and mantle viscosity for northern Europe. Geophys. J. Int. 134, 102–144.
Larsen, N.K., Linge, H., Hakansson, L., Fabel, D., 2012. Investigating the last deglaciation of the Scandinavian Ice Sheet in southwest Sweden with Be-10 exposure dating. J. Quat. Sci. 27, 211–220.
Lecavalier, B., Milne, G.A., Simpson, M.J.R., Wake, L., Huybrechts, P., Tarasov, L., Kjeldsen, K.K., Funder, S., Long, A.J., Woodroffe, S., Dyke, A.S., Larsen, N.K., 2014. A model of Greenland ice sheet deglaciation constrained by observations of relative sea level and ice extent. Quat. Sci. Rev. 102, 54–84.
Lifton, N., Smart, D.F., Shea, M.A., 2008. Scaling time-integrated in situ cosmogenic nuclide production rates using a continuous geomagnetic model. Earth Planet. Sci. Lett. 268, 190–201.
Lundqvist, J., 1986. Late Weichselian glaciation and deglaciation in Scandinavia. Quat. Sci. Rev. 5, 269–292.
Lundqvist, J., Wohlfarth, B., 2001. Timing and east–west correlation of south Swedish ice marginal lines during the Late Weichselian. Quat. Sci. Rev. 20, 1127–1148.
Lunkka, J.P., Johansson, P., Saarnisto, M., Sallasmaa, O., 2004. Glaciation of Finland. In: Ehlers, J., Gibbard, P.L. (Eds.), Developments in Quaternary Sciences. Elsevier, Amsterdam, The Netherlands, pp. 93–100.
Marcott, S.A., 2011. Late Pleistocene and Holocene Glacier and Climate Change, Geosciences. Oregon State University, Corvallis, p. 266.
Marcott, S.A., Shakun, J.D., Clark, P.U., Mix, A.C., 2013. A reconstruction of regional and global temperature for the past 11,300 years. Science 339, 1198–1201.
Mauz, B., Ruggieri, G., Spada, G., 2015. Terminal Antarctic melting inferred from a far-field coastal site. Quat. Sci. Rev. 116, 122–132.
Mitrovica, J.X., Davis, J.L., Shapiro, I.I., 1994. A spectral formalism for computing 3-dimensional deformations due to surface loads. 1. Theory. J. Geophys. Res., Solid Earth 99, 7057–7073.
Mitrovica, J.X., Wahr, J., Matsuyama, I., Paulson, A., 2005. The rotational stability of an ice-age earth. Geophys. J. Int. 161, 491–506.
Paterson, W.S.B., 1972. Laurentide Ice Sheet: estimated volumes during late Wisconsin. Rev. Geophys. Space Phys. 10, 885–917.
Paulson, A., Zhong, S., Wahr, J., 2005. Modelling post-glacial rebound with lateral viscosity variations. Geophys. J. Int. 163 (1), 357–371.
Peltier, W.R., 2004. Global glacial isostasy and the surface of the ice-age earth: the ice-5G (VM2) model and grace. Annu. Rev. Earth Planet. Sci. 32, 111–149.
Peltier, W.R., Argus, D.F., Drummond, R., 2015. Space geodesy constrains ice age terminal deglaciation: the global ICE-6G_C (VM5a) model. J. Geophys. Res. 120 (1), 450–487.
Rasmussen, S.O., Andersen, K.K., Svensson, A.M., Steffensen, J.P., Vinther, B.M., Clausen, H.B., Siggaard-Andersen, M.L., Johnsen, S.J., Larsen, L.B., Dahl-Jensen, D., Bigler, M., Rothlisberger, R., Fischer, H., Goto-Azuma, K., Hansson, M.E., Ruth, U., 2006. A new Greenland ice core chronology for the last glacial termination. J. Geophys. Res., Atmos. 111.
Rinterknecht, V.R., Clark, P.U., Raisbeck, G.M., Yiou, F., Bitinas, A., Brook, E.J., Marks, L., Zelcs, V., Lunkka, J.P., Pavlovskaya, I.E., Piotrowski, J.A., Raukas, A., 2006. The last deglaciation of the southeastern sector of the Scandinavian Ice Sheet. Science 311, 1449–1452.
Ross, M., Utting, D.J., Lajeunesse, P., Kosar, K.G.A., 2012. Early Holocene deglaciation of northern Hudson Bay and Foxe Channel constrained by new radiocarbon ages and marine reservoir correction. Quat. Res. 78, 82–94.
Shakun, J.D., Clark, P.U., He, F., Lifton, N.A., Liu, Z., Otto-Bleisner, B.L., 2015. Regional and global forcing of glacier retreat during the last deglaciation. Nat. Commun. 6.
Shakun, J.D., Clark, P.U., He, F., Marcott, S.A., Mix, A.C., Liu, Z.Y., Otto-Bliesner, B., Schmittner, A., Bard, E., 2012. Global warming preceded by increasing carbon dioxide concentrations during the last deglaciation. Nature 484, 49–55.
Simon, K.M., James, T.S., Forbes, D.L., Telka, A.M., Dyke, A.S., Henton, J.A., 2014. A relative sea-level history for Arviat, Nunavut, and implications for Laurentide Ice Sheet thickness west of Hudson Bay. Quat. Res. 82, 185–197.
Staiger, J., Gosse, J., Toracinta, R., Oglesby, B., Fastook, J., Johnson, J.V., 2007. Atmospheric scaling of cosmogenic nuclide production: climate effect. J. Geophys. Res., Solid Earth 112.
Stone, J.O., 2000. Air pressure and cosmogenic isotope production. J. Geophys. Res. 105, 23,753–723,759.
Stroeven, A.P., Fabel, D., Harbor, J.M., Fink, D., Caffee, M.W., Dahlgren, T., 2011. Importance of sampling across an assemblage of glacial landforms for interpreting cosmogenic ages of deglaciation. Quat. Res. 76, 148–156.
Stroeven, A.P., Hattestrand, C., Kleman, J., Heyman, J., Fabel, D., Fredin, O., Goodfellow, B.W., Harbor, J.M., Jansen, J.D., Olsen, L., Caffee, M.W., Fink, D., Lundqvist, J., Rosqvist, G.C., Stromberg, B., Jansson, K.N., 2015a. Deglaciation of Fennoscandia. Quat. Sci. Rev. http://dx.doi.org/10.1016/j.quascirev.2015.09.016.
Stroeven, A.P., Heyman, J., Fabel, D., Björck, S., Caffee, M.W., Fredin, O., Harbor, J.M., 2015b. A new Scandinavian reference ^{10}Be production rate. Quat. Geochronol. 29, 104–115.
Svendsen, J.I., Briner, J.P., Mangerud, J., Young, N.E., 2015. Early break-up of the Norwegian Channel Ice Stream during the Last Glacial Maximum. Quat. Sci. Rev. 107, 231–242.
Tarasov, L., Dyke, A.S., Neal, R.M., Peltier, W.R., 2012. A data-calibrated distribution of deglacial chronologies for the North American ice complex from glaciological modeling. Earth Planet. Sci. Lett. 315, 30–40.
Ullman, D.J., 2013. Dismantling the Laurentide Ice Sheet: refining the chronology and mechanisms of deglaciation. Geosciences. University of Wisconsin–Madison, p. 220.
van der Wal, W., Whitehouse, P.L., Schrama, E.J.O., 2015. Effect of GIA models with 3D composite mantle viscosity on GRACE mass balance estimates for Antarctica. Earth Planet. Sci. Lett. 414, 134–143.
Velicogna, I., Sutterley, T.C., van den Broeke, M.R., 2014. Regional acceleration in ice mass loss from Greenland and Antarctica using GRACE time-variable gravity data. Geophys. Res. Lett. 41, 8130–8137.
Whitehouse, P.L., Bentley, M.J., Le Brocq, A.M., 2012. A deglacial model for Antarctica: geological constraints and glaciological modelling as a basis for a new model of Antarctic glacial isostatic adjustment. Quat. Sci. Rev. 32, 1–24.
Wohlfarth, B., Björck, S., Funder, S., Houmark-Nielsen, M., Ingólfsson, O., Lunkka, J.P., Mangerud, J., Saarnisto, M., Vorren, T., 2008. Quaternary of Norden. Episodes 31, 73–82.
Wu, P., Van der Wal, W., 2003. Postglacial sea-levels on a spherical, self-gravitating viscoelastic earth: effects of lateral viscosity variations in the upper mantle on the inference of viscosity contrasts in the lower mantle. Earth Planet. Sci. Lett. 211, 57–68.
Young, N.E., Schaefer, J.M., Briner, J.P., Goehring, B.M., 2013. A Be-10 production-rate calibration for the Arctic. J. Quat. Sci. 28, 515–526.
Zwally, H.J., Li, J., Robbins, J.W., Saba, J.L., Yi, D., Brenner, A.C., 2015. Mass gains of the Antarctic ice sheet exceed losses. J. Glaciol. 61, 1019–1036.